JAAS

PAPER

View Article Online
View Journal | View Issue

Cite this: J. Anal. At. Spectrom., 2016, 31, 994

Ultratrace analysis of krypton isotopes by resonant ionization spectroscopy-time of flight mass spectrometry (RIS-TOF)

Eric Gilabert,*[ab] Bernard Lavielle,[ab] Bertrand Thomas,[ab] Sylvain Topin,[c] Fabien Pointurier[c] and Christophe Moulin[c]

Received 23rd October 2015
Accepted 25th February 2016

DOI: 10.1039/c5ja00423c

www.rsc.org/jaas

A new RIS-TOF instrument, called FAKIR (Facility for Analyzing Krypton Isotope Ratios), has been developed at CENBG in order to measure Kr isotope ratios with an extremely high sensitivity. The instrument uses a single color Kr ionization scheme with tunable coherent UV photons near 216.6 nm. A two-photon resonance excitation allows it to reach the $5p[5/2]_2$ excitation level followed by a single-photon ionization. Krypton ions are accelerated towards an electron multiplier. The instrument includes a cryogenic concentrator that increases the efficiency of the ion source and a new selecting system allowing the deflection of the abundant isotopes before they impact the detector. This device eliminates the blinding effect on the detector that alters the detection of the less abundant Kr isotopes. The current sensitivity of the instrument of ~6700 atoms has been demonstrated by extracting the gas from 37 mg of the Boguslavka iron meteorite. The associated errors on the ^{81}Kr isotope ratio measurements did not exceed ~12%. A good agreement is observed with conventional mass spectrometry analysis, which requires several grams of material, by measuring the cosmic ray exposure age of the Boguslavka meteorite.

1. Introduction

For almost 50 years the measurement of radioactive Kr isotopes has attracted great interest as tracers for dating environmental samples.[1] Essentially produced by nuclear reactions induced by cosmic ray secondary neutrons, ^{81}Kr concentration is stable in the atmosphere, short-term fluctuations in production due to variations of the cosmic ray intensity being smoothed out.[2,3] Moreover, ^{81}Kr is chemically inert as an isotope of a noble gas and its underground production is negligible.[4] With a half-life of 229 000 years it is considered as one of the best tracers for groundwater and ice core dating in the time range 50 000 to 800 000 years. Krypton-85 with a half-life of 10.7 years is released in the atmosphere during the reprocessing of nuclear fuel. As a consequence, its average concentration in the atmosphere is reasonably known for several decades. Therefore ^{85}Kr can also be used for dating "young" groundwaters and for tracing anthropogenic nuclear activities in the atmosphere. In the field of cosmochemistry, the dating method based on the measurement of ^{81}Kr coupled with several other stable Kr isotopes (*ca.* ^{80}Kr, ^{82}Kr, ^{83}Kr) in meteorites is considered as the most reliable method to determine the exposure time of these extra-terrestrial objects to galactic cosmic rays in space. Such data are important for studying the collisional history of their parent bodies[5] and the dynamic evolution of planetary surfaces like the Moon and Mars.[6]

Due to the extremely low abundance of ^{81}Kr and ^{85}Kr in environmental samples, the resonance ionization source (RIS) has rapidly become one of the most promising detection techniques. Several instrumental developments have occurred over the last 30 years in particular with regard to efficient ion sources based on the multi resonant scheme using several wavelengths.[7–9] Such an approach leads to a complex set-up requiring in particular the simultaneous use of several tunable laser beams.[10]

The ionization method developed in this work is based on a single color 2 + 1 photons ionization scheme which is much easier to implement. The facility named FAKIR for Facility for Analyzing Krypton Isotope Ratios also includes a cryogenic concentrator to increase the ionization efficiency and a time of flight mass analyser.

Before admitting gas sample within the instrument, specific Kr extraction and purification processes are generally required including an isotope enrichment step as described by Lavielle *et al.*[11] This is especially needed when the ratio of stable Kr isotopes to radio-krypton isotope is very large (*i.e.* $>10^3$ as for groundwater, ice core, Earth atmosphere). On the contrary, Kr production induced by cosmic rays in space can be directly investigated in many small meteorite samples (10–20 mg) after a rapid cleaning of the extracted gases.

[a]University of Bordeaux, CENBG, UMR 5797, Gradignan, France. E-mail: gilabert@cenbg.in2p3.fr
[b]CNRS, IN2P3, CENBG, UMR 5797, Gradignan, France
[c]CEA, DAM, DIF, F-91297 Arpajon, France

2. Experimental set-up and performance

The experimental set-up (Fig. 1) consists of an ionizing laser, a heating laser, a cold trap, a time of flight mass spectrometer with an ion deflecting system, an ion multiplier as a detector coupled with a digital oscilloscope. This set-up is largely inspired from the ones developed by Thonnard *et al.*[12] and Gilmour *et al.*[13] The ion deflecting system is a new device specially designed at CENBG for Kr trace measurements when Kr isotope abundances show large dynamics (>10^3).

2.1 Ionizing laser

Several resonance ionization schemes have been investigated for Kr atoms, including single and two-photon resonance excitations.[12,14,15] Since the noble gas atoms require high energy (around 10 eV or more) for the transition from the ground state, it is rather challenging to obtain sufficient laser output using commercially available lasers with corresponding single-photon resonance wavelength. Therefore the resonant "2 + 1" transition, a two-photon resonance excitation followed by a single-photon ionization at the same wavelength was selected as shown in Fig. 2.[16] The wavelength used is 216.603 nm allowing it to reach with 2 photons, the $5p[5/2]_2$ excited state. This state is not the lowest in energy but it can be easily reached with a very good yield using a common R6G dye laser. The third photon is not resonant, but its energy is high enough to complete the ionization of the Kr atom.

An injected Nd:YAG laser (PW8010, Continuum) supplies 1.6 J at 1064 nm with a small bandwidth (<0.003 cm^{-1}). The light is frequency doubled and tripled with energies around 600 mJ and 300 mJ, respectively. The doubled frequency light is used to pump a dye laser ('Narrow Scan' from Radiant Dye, bandwidth < 0.06 cm^{-1}) that produces photons at 557 nm with energies of 100 mJ. This light is then mixed with the tripled frequency in BBO (beta-barium borate) crystals and produces photons around 216 nm with energies of 10 mJ and pulse duration around 10 ns with a 10 Hz repetition rate. This laser light is then focused in the ionization chamber by a 150 mm lens.

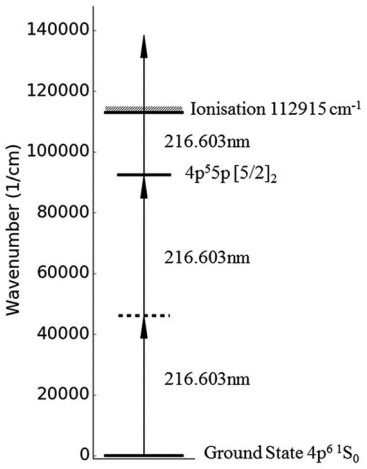

Fig. 2 Kr ionization scheme.

2.2 TOF source and cold trap

The design of the source was made using the SIMION® code. Initially, three plates are used to accelerate and focus the Kr beam in the spectrometer. The first plate is the cold trap. The following plates are positioned at 0.4 cm, and 4.6 cm from the cold trap. They are provided with two holes, a 1 cm-diameter in the ion beam path in the center and another one, on the side to allow the heating laser beam to reach the cold trap. Voltage is

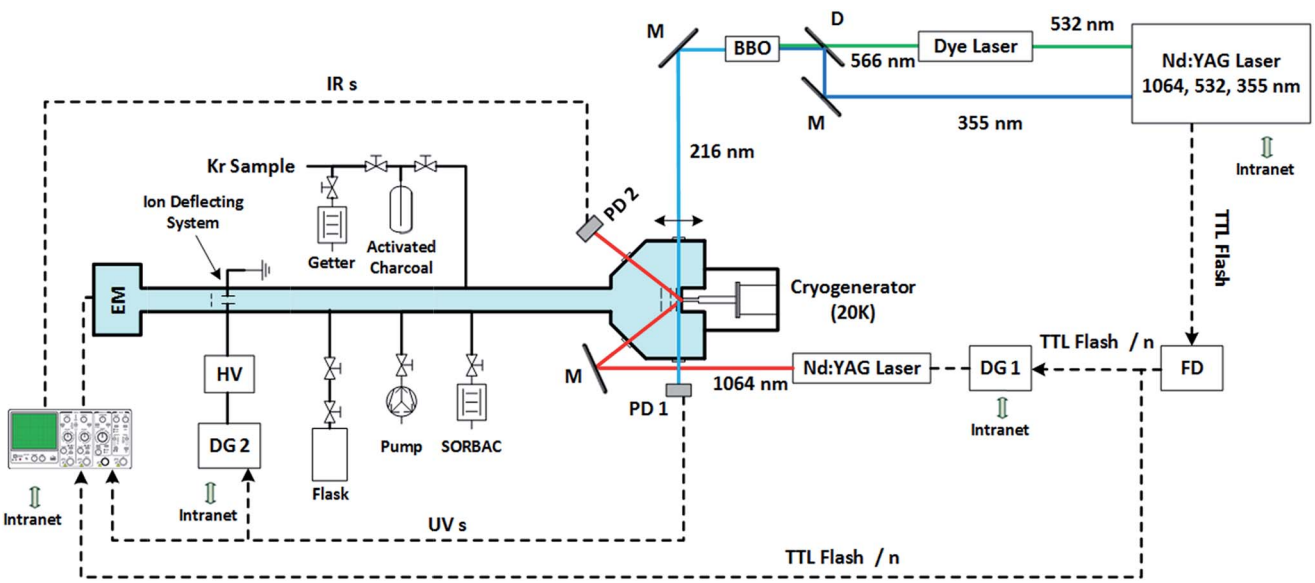

Fig. 1 Experimental set-up. M: mirror, D: dichroic, FD: frequency divider, DG: delay generator, PD: photodiode, EM: electron multiplier. HV: rapid high voltage. Flask: air standard calibration. IRs, UVs: infrared, UV photodiode signals. SORBAC®: gas purification.

typically 1000 V for the cold trap and 900 V for the second plate. The last plate is at ground. The small distance and difference voltage between the first and second plate allow a good focusing of the ion beam. To simulate the beam, Kr atoms are ionized in a small volume near the cold trap with a cylindrical shape in the UV laser direction. These simulations have shown that there is no important constraint in the geometry and in the voltage for the ionized atoms to reach the detector. The total length of the flying tube is 90 cm. Detection is performed by an ion multiplier model FastTof (14880) from SGE Ltd. (UK) specially designed for time of flight experiments. Even if MCP (Multi-Channel Plate) are more usual detectors for time of flight mass spectrometry, this ion multiplier detector gives also satisfying linearity, sensibility and noise properties with lower cost.

The signal is triggered by the UV photodiode and recorded on a digital oscilloscope (TDS5104 from Tektronix). In order to improve the ionization efficiency, an atom buncher following the principle first described by Hurst *et al.*[17] and Lehmann *et al.*[18] is used. The design of the cold trap used in this work (see Fig. 3) is largely inspired by Gilmour *et al.*[13] By using a very thin stainless steel foil (about 50 μm thickness) in contact with a 2 mm-diameter copper rod cooled at 50 K by a commercial cold generator from Cryodynes, it is possible to create a large thermal gradient (about 100 K mm^{-1}) allowing the condensation of Kr atoms on a small spot. Kr atoms can be released by heating the cold spot. Therefore the probability to ionize the Kr atoms and then the sensitivity of the apparatus are locally increased. The difficulty of such a set-up is that the cold trap must also be maintained at a high voltage (about 1000 V) for the extraction and acceleration of the ions. A sapphire disk as shown on Fig. 3 (item 8), is used to give both proper electrical insulation and good thermal transfer. An indium foil is added between the copper finger and stainless steel surface to improve the quality of the contact and then the thermal transfer (item 2). A stainless steel spring (item 7) ensures the contact between the thin stainless steel foil and the end of the copper rod after the thermal contraction at low temperature.

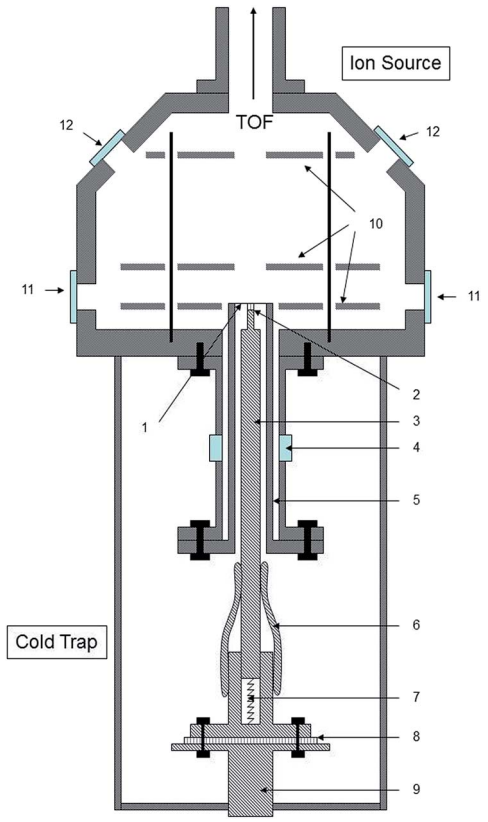

Fig. 3 Schematic of the cold trap and ion source: 1 – thin stainless-steel end, 2 – indium, 3 – copper insert, 4 – insulating ceramic, 5 – re-entrant tube, 6 – copper heat wick, 7 – spring, 8 – insulating sapphire, 9 – cold head, 10 – electrostatic plates, 11 – UV view ports, 12 – IR view ports.

2.3 Heating laser

The heating laser is a Nd:YAG (Ultra from Big Sky Laser) that can deliver up to 50 mJ at 1.064 μm. However, the analytical method described in this paper requires only 1 mJ. The heating laser is used only for controlled energy surface deposit and not for the light properties. The atom desorption is mainly driven by the laser pulse duration and the surface temperature.[13] The heating laser beam enters the chamber and reaches the cold trap under a 45° angle. A fraction of the light is reflected and goes out through another window. The detection of light is carried out for adjusting the reference time delay. The beam size at the cold spot position is about 5 mm in diameter, as compared to the 2 mm large cold trap disk, to avoid any permanent trapping of Kr.

Delays between Kr ionization and heating pulses are controlled by a pulse delay generator (BNC 555). A flash TTL signal with a frequency of 10 Hz from the PW8010 Nd:YAG laser triggers the pulse delay generator. A frequency divider has been added between the PW8010 and the delay generator, to slow down the desorption rate process from 10 Hz to 0.1 Hz in order to increase the Kr trapping time on the cold spot between two laser shots. The coordination of the two lasers, referred to as 'inter-laser delay' is controlled by two photodiodes placed in the exiting UV beam from the ionization chamber and in the IR beam after reflecting on the cold trap, respectively. The zero time delay is set when the two pulses are in coincidence.

2.4 Ion deflection system

The ion deflection system is a new development included in the TOF tube to selectively reject undesired Kr ions. The purpose is to eliminate one or more Kr isotopes during travel from the source to the detector using an electrostatic high-voltage. Such a device avoids a blinding effect on the detector due to the impact of a large number of ions at mass M (^{80}Kr or ^{84}Kr) before detecting a very small signal at mass $M + 1$ (^{81}Kr or ^{85}Kr). The design of the deflecting system and also an update of the source were made with the SIMION® code. The deflecting is sensitive to the length and the aperture of the electrostatic field. A fourth plate and a steerer have been added in the source to correct the misalignment and to focus the beam in the region of the deflecting system. The set-up includes two electrostatic plates (length and space in between are 5 mm), a pulse generator (Quantum 9514) and a fast high-voltage amplifier (DEI

PVM4210). This amplifier provides 900 V positive and negative voltages with a rise-time and a down-time of 5 ns. An X–Y adjustable diaphragm is placed between the plates and the detector to stop deflected ions. By optimizing the design of the plates taking into account the beam properties, this device allows eliminating any of the Kr isotopes without disturbing the adjacent ones. Fig. 4 presents two Kr spectra obtained by analyzing a small Kr sample of air composition with and without the deflecting device. The dotted line is without voltage. The solid line is when +600 V and −600 V are simultaneously applied respectively on the two deflecting plates by a pulse of 40 ns that corresponds to the shortest possible time required to obtain the full voltage on the plates. The targeted ^{83}Kr signal completely disappears, and a small change in peak shape is only observed that does not modify isotopic ratios. Taken into account the rise-time of high-voltage, and the fringe electric field outside of the deflecting plates, the effective deflecting time is 160 ns. This is consistent with operation of the system because the width at the base of a peak is 40 ns and the time span between two adjacent masses is 110 ns and then 220 ns between the $M-1$ and $M+1$. The high-voltage is switched on only 10 ns after the end of the previous peak $(M-1)$. The delay between the return to the zero voltage and the next peak arrival $(M+1)$ is also 10 ns. Therefore the start and the end of the high-voltage can be easily and exactly adjusted between two peaks and ions can be removed without modifying the peaks to detect.

2.5 Correction of the mass discrimination

Mass discrimination can have several origins: a systematic difference in the ionization of the Kr isotopes, space charge effects in the ion source and a difference in detection efficiency. To determine this parameter, 25 air standards were analyzed with the RIS-TOF before the meteorite sample. The parameter $d = R_{mes}/R_t - 1$ is used to characterize the isotopic effect on the measurement, where R_{mes} is the ratio determined with our instrument and R_t the ratio in air.[19] Measurements correlated well with the mass of the isotope, and this allows us to define the discrimination per unit of atomic mass as $MD = d/(M_{ref} - M_{mes})$, where M_{ref} is the mass of the reference isotope and M_{mes} is the mass of the isotope of interest. The mean measured isotopic ratios obtained for ^{80}Kr/^{86}Kr, ^{82}Kr/^{86}Kr, ^{83}Kr/^{86}Kr and ^{84}Kr/^{86}Kr are respectively 0.1378 ± 0.0027, 0.7137 ± 0.0085, 0.6991 ± 0.0087 and 3.311 ± 0.016. For MD (in % per a.m.u.) we obtained 1.04 ± 0.35, 1.94 ± 0.32, 1.84 ± 0.44 and 0.54 ± 0.24 respectively. The adopted MD (% per a.m.u.) value is then 1.5 ± 0.5%.

2.6 Optimization of the heating laser parameters

Two parameters of the heating laser have a major influence on the analytical performance of the system: the inter-laser delay and the repetition rate. Fig. 5 shows the Kr signal intensity *versus* the inter-laser delay. The zero delay is obtained when both UV and IR laser signals recorded by the two photodiodes are coincident. The UV signal is filtered and detected after transmission through the ionization chamber. The IR signal is a reflecting light from the cold zone. As shown in Fig. 5, the time required for desorbing Kr atoms from the cold trap and to move to the ionization zone 0.5–1.5 mm above is 1.5 μs. Regarding the repetition rate, two modes are used, a normal mode at 10 Hz and a slow mode at 1 Hz. At 10 Hz we estimate that about 2% of the total Kr atoms present in the mass spectrometer are trapped between two laser shots. At 1 Hz, the trapping efficiency appears to be an order of magnitude better. As a consequence, the slow mode significantly increases the signal to noise ratio. As expected, the laser heating intensity also plays an important role. Tests show first an increase of the ionization efficiency with the laser intensity followed by a sudden decrease of the ionization efficiency. This is likely to be attributed to the vaporization of the metal surface that inhibits the ionization process.

2.7 Influence of the ionization laser wavelength

Fig. 6 shows the influence of the ionization laser wavelength on the $^{84}Kr^+$ signal. Wavelengths taken into account are those generated by the dye laser after mixing with the third harmonic

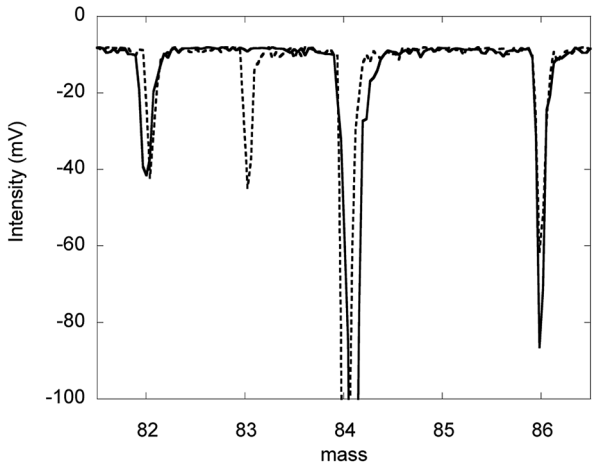

Fig. 4 Spectra of an atmospheric Kr sample obtained without deflecting voltage (dashed line) and with deflecting voltage (solid line) applied to ^{83}Kr.

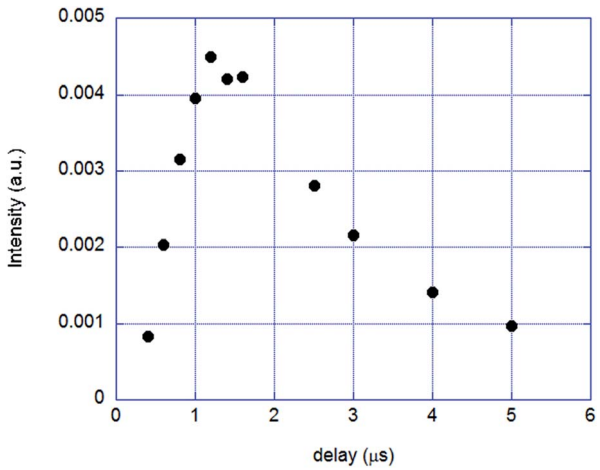

Fig. 5 Kr signal intensity against the inter-laser delay. The maximum ionization is obtained for a delay of 1.5 μs.

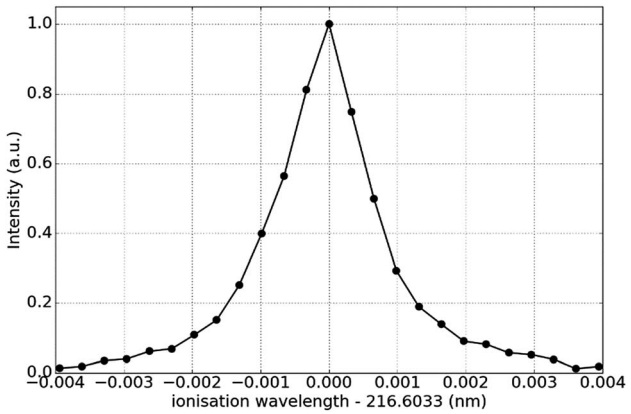

Fig. 6 Influence of the ionization laser wavelength on the $^{84}Kr^{+}$ signal.

of the Nd:YAG laser. Maximum ionization is obtained at 556.425 nm for the dye laser. After mixing with the 355 nm wavelength, the UV wavelength is 216.6033 nm. With a two-photon ionization process, the corresponding level is 108.3016 nm (11.4559 eV). The excited state $5p[5/2]_2$ is given at 11.4447 eV.[20] The very small difference is probably due to an inaccurate calibration of the controller of the dye laser. The accuracy of the isotopic ratios does not allow for seeing ionization hyperfine effects on Kr isotopes[21] and are included in statistical errors.

2.8 Calibration and performance

A 2 liter calibration container is filled with air after removing N_2, O_2 using Ti sponges and SORB-AC® getters, and Ar by cryogenic distillation. The gas volume was first fractionated several times using precisely calibrated volumes until appropriate Kr quantities are obtained according to RIS-TOF sensibility. Sensitivity and mass discrimination are measured by analyzing 0.8 cm^3 of air sampled into the calibration container, corresponding to 10^6 atoms of Kr.

After determining the main operating parameters (UV wavelength, delays, optical alignment, IR and UV intensities), the -TOF sensitivity, its detection limit (lowest content that can be measured with reasonable statistical certainty) and the mass discrimination must be characterized. In addition, the effects of the concentration of the analyzed gas and the detector gain can be studied.

Krypton standards with air composition are introduced into the instrument with various concentrations, and using different settings and electron multiplier detector (EM) gains. For the highest EM gains (90–100% of the 3 kV recommended maximum voltage), tests have highlighted nonlinear effects. However, a linear range is obtained for signals smaller than 500 mV. For lower gains (between 50% and 80% of the maximum voltage), the linear range is extended to signals higher than 500 mV. As a consequence to minimize these effects, the EM gain is adjusted or the gas is fractionated so that the highest signal does not exceed 500 mV. The detection limit is usually given as twice the noise signal. The sensitivity is the ratio of the number of atoms to the peak area of the mass under consideration. It is expressed in atoms per (mV μs). Because the shapes of the peaks are quite reproducible, we can also characterize the sensitivity as the ratio of the number of atoms to the maximum value of the peak in mV (corrected for the baseline). It is then expressed in atoms per mV. This sensitivity is less accurate but more suitable and more readable for the test phases and settings. The sensitivity and the noise signal depend on the gain applied, the settings and alignment conditions that can fluctuate from one day to the other. However, no clear dependence on isotope ratios have been detected for different conditions (settings, gain, and concentration). In the best case, the sensitivity is around 1000 atoms per mV and the detection limit ~0.5 mV or ~500 atoms. Repeated calibration measurements generally show on the same day sensitivity variations within 10%. The purpose of this instrument is primarily the determination of the isotopic ratio $^{81}Kr/^{83}Kr$ at very low concentration. When precise absolute calibration determination is required, we plan to achieve an isotope dilution procedure using an isotopically enriched Kr spike.

2.9 Software

In-house developed software created using Labview® is implemented for operating FAKIR. All devices (delay generators, YAG and dye laser controls, digital oscilloscope) are connected to the laboratory's internal network *via* serials and TCP/IP servers. A first control-software tunes the dye laser for wavelength and automated tracking. A second one pilots the delay generators. The last one drives the digital oscilloscope. Every 100 ms, a Kr spectrum is recorded on a computer. The software displays the mean of the last 10 spectra and the mean of all recorded spectra. Information like position, amplitude peak and ratios can be monitored in real-time during analysis. Another control-software is used at the end of the experiment to compile all the spectra and determine Kr isotopes amplitude evolution and isotopic ratios.

2.10 Analysis

The different steps of an analysis are:

(1) The gas is allowed time to expand in the entire volume of the RIS-TOF.

(2) 2% to 20% (depending on the laser repetition rate) of the Kr atoms are trapped on the cold spot between two consecutive heating laser fires.

(3) Kr atoms are released from the cold spot by a shot from the heating laser.

(4) 1.5 μs later, the UV laser is fired and Kr atoms are ionized in the laser beam-waist if the power density is sufficient. This laser shot also triggers the acquisition of the digital oscilloscope with the use of a photodiode.

(5) Ionized atoms are accelerated by the source.

(6) Kr isotopes are deflected or trapped in-flight by the deflecting system.

(7) The digital oscilloscope records the waveform and transfers it to the computer without any treatment.

(8) Back to step 2 at the chosen repetition rate or stop if an adequate signal/noise ratio is reached.

(9) Waveforms are then treated to monitor isotopic ratios and peak intensities.

3. Application to the Boguslavka iron meteorite

3.1 Sample and experimental

Boguslavka is an iron meteorite classified as IIAB-type felt in Russia in 1916. The total recovered mass was 256 kg. 3.27 grams had been sampled in the main mass from the Smithsonian Institution collection (USMN-1374). Boguslavka sample has been analyzed first by conventional mass spectrometry (MS) and then by RISTOF techniques. Results obtained with both methods are presented here. MS needs more matter because its sensitivity is 20–50 times lower than RISTOF. The experimental set-up of the conventional MS technique, already used for measuring ^{81}Kr in extraterrestrial matter at CENBG, is described elsewhere.[22] The analysis line is composed of a baking sample storage area, a gas extraction line including an electron impact vacuum furnace that reaches 2000 °C, an introduction line with Ti sponge and SORBAC® getters (SAES Getter) allowing gas purification and finally a mass spectrometer. The latter includes a Nier-type source, a 12 cm radius 60° magnet and an ion multiplier connected to a pico-ampere-meter (Keithley 6485). The system also includes active charcoals for transferring heavy noble gases (Ar, Kr, Xe) from one line to the other ones by cryogenic trapping. The high vacuum is ensured by a turbo-molecular pump and three ionic pumps that maintain a pressure better than 10^{-9} mbar. Small parts of the sample are prepared by means of a water-cooled diamond wire saw and introduced in to the storage device and baked for a few days at 60–80 °C to remove atmospheric surface contamination. Finally, they are completely melted and analyzed by MS or the RIS-TOF technique. System blank analysis and calibrations are regularly performed before and after each analysis. For MS, 800–1000 mg are necessary to measure ^{81}Kr/Kr isotope ratios with a relative precision better than 10%. The results of MS measurements are reported in Table 1.

For RIS-TOF experiments, only a few tens of mg are used. After complete melting of the sample, the released gas is purified with chemical traps to remove excess of N_2, O_2 and H_2 in the lines. The gas is then split in two fractions. The lowest fraction (20%) is used for measuring the isotopic composition for stable isotopes (^{78}Kr, ^{80}Kr, ^{82}Kr, ^{83}Kr, ^{84}Kr, and ^{86}Kr). The gain of the detector is carefully adjusted to ensure linearity. The largest fraction is for measuring precisely the isotopic ratio ^{81}Kr/^{78}Kr. The gain of the detector is optimized for ^{78}Kr measurement. Data acquisition is performed for 10–15 min with a spectrum collected every minute. This procedure allows us to follow the intensity and isotope ratio evolution with time in order to determine both values at the starting time of the measurements. This temporal evolution is correlated to the fluctuations of the laser intensity that induce variable ionization rates and signal intensities. A weak memory effect can also be observed, leading to an increase of the signal intensities over time. However, isotope ratio measurements are only slightly affected by ionization rate or memory effect and are corrected if necessary. Typical results with a 1 minute acquisition time are presented in Fig. 7a.

Baseline subtraction is performed independently for each isotope. Baselines are determined by fitting the two sides of the peak with an analytical function. Most of the time, the mean value between left and right sides is sufficient. However, for a small signal (typically for ^{81}Kr), linear or polynomial functions are necessary. The sensitivity of the whole analytical line allowed the measurement of ~6700 atoms of ^{81}Kr (signal of 4 mV). The detection limit is defined as twice the amplitude of the noise (*i.e.* 0.5 mV) and is ~1500 atoms. The absence of detectable peaks at masses 77 and 79 (Fig. 7b), customarily used to monitor possible hydrocarbon contaminations, indicates there is presumably no hydrocarbons at the neighbor masses of interest (78 and 81). Blanks of the analytical lines are also measured regularly, showing that no ^{81}Kr is detectable and that correction is less than 1% for the major isotopes. Krypton isotope ratios and ^{83}Kr concentrations are also reported in Table 1. The averaged relative uncertainties for isotopic ratios (excepted ^{81}Kr/^{83}Kr) are ~2%. Relative uncertainty on the ^{81}Kr/^{83}Kr ratio is 10%.

3.2 Cosmogenic component

The data are consistent with a two-component mixing between cosmogenic Kr and trapped Kr of composition corresponding to the terrestrial atmosphere. The so-called cosmogenic component is the result of irradiation of the cosmic object by galactic or solar radiation particles of trace elements such as Zr, Mo or Ru. The most produced Kr isotope by these spallation reactions is ^{83}Kr. Production rates decrease slowly for lighter isotopes. On the heavier isotope side, production falls very quickly to zero for ^{86}Kr.[23] In Fig. 7a, there is a significant enrichment in light isotopes notably for ^{78}Kr and ^{80}Kr relative to the Kr air

Table 1 ^{83}Kr concentrations in 10^{-12} cm^3 g^{-1} STP and isotopic ratios in samples from the Boguslavka meteorite analyzed by conventional mass spectrometry (MS) and RIS-TOF. Uncertainties correspond to one sigma error

Sample	Mass (g)	Method	^{83}Kr	^{78}Kr/^{83}Kr ≡ 1	^{80}Kr	^{81}Kr	^{82}Kr	^{84}Kr	^{86}Kr
Bogu 2.3	0.7037	MS	2.180	0.3080	0.6148	0.00438	0.9066	0.710	0.1703
			±0.089	±0.0042	±0.0093	±0.00026	±0.0189	±0.016	±0.0080
Bogu 3.1	0.7377	MS	2.378	0.2728	0.5610	0.00337	0.9042	1.231	0.3525
			±0.098	±0.0033	±0.0044	±0.00013	±0.0049	±0.015	±0.0061
Bogu 4	0.0370	RIS-TOF	3.51	0.2366	0.5002	0.00247	0.9432	2.016	0.6286
			±0.35	±0.0113	±0.0144	±0.00030	±0.0093	±0.030	±0.020

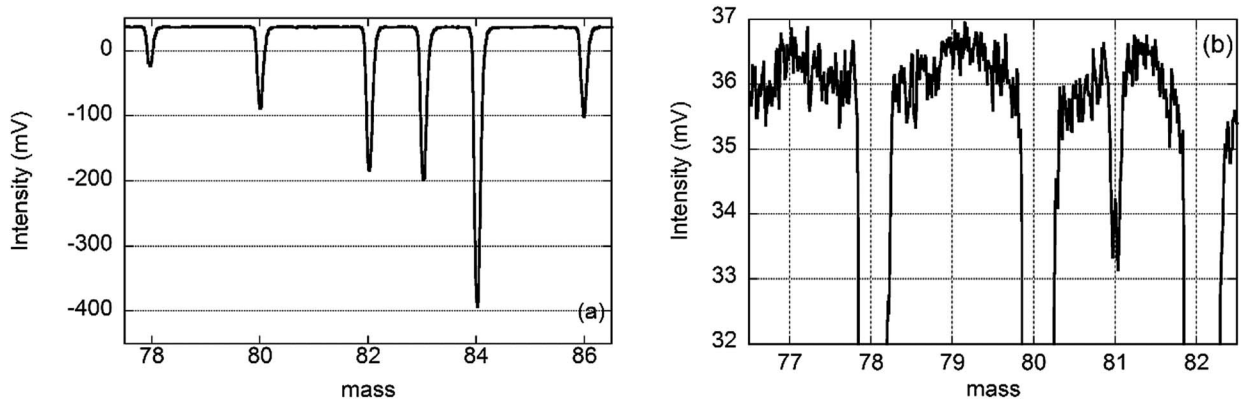

Fig. 7 (a) Kr spectra of the Boguslavka meteorite obtained with 20% of the released gas. Gain is divided by 2 compared to (b) to ensure a signal less than 500 mV and linearity (b) zoom on the ^{81}Kr signal from 80% of the released gas. The ^{81}Kr signal corresponds to ~6700 atoms and the noise amplitude is ~750 atoms.

composition. The peak of the ^{86}Kr is purely atmospheric as well as most of the ^{84}Kr peak. Krypton cosmogenic concentrations and isotope ratios can be deduced from the assumption that all ^{86}Kr belongs to the trapped component, which is here assumed to be air. Atmospheric composition for other isotopes is also preserved. The isotopic ratios and the cosmogenic concentrations can be calculated using the measured values and atmospheric ratios.[19]

In the following equations, "m" refers to the measured value, "c" refers to the cosmogenic component, "a" is the component trapped in the meteorite that we take to the terrestrial atmospheric component.

Cosmogenic ^{83}Kr concentration can be expressed as:

$$[^{83}\mathrm{Kr}]_c = [^{83}\mathrm{Kr}]_m \left(1 - \frac{\left(\frac{^{86}\mathrm{Kr}}{^{83}\mathrm{Kr}}\right)_m}{\left(\frac{^{86}\mathrm{Kr}}{^{83}\mathrm{Kr}}\right)_a}\right) \quad (1)$$

For cosmogenic isotope ratios (n = 78, 80, 82 and 84):

$$\left(\frac{^{n}\mathrm{Kr}}{^{83}\mathrm{Kr}}\right)_c = \frac{\left(\frac{^{n}\mathrm{Kr}}{^{83}\mathrm{Kr}}\right)_m \times \left(\frac{^{86}\mathrm{Kr}}{^{83}\mathrm{Kr}}\right)_a - \left(\frac{^{n}\mathrm{Kr}}{^{83}\mathrm{Kr}}\right)_a \times \left(\frac{^{86}\mathrm{Kr}}{^{83}\mathrm{Kr}}\right)_m}{\left(\frac{^{86}\mathrm{Kr}}{^{83}\mathrm{Kr}}\right)_a - \left(\frac{^{86}\mathrm{Kr}}{^{83}\mathrm{Kr}}\right)_m} \quad (2)$$

with $(^{81}\mathrm{Kr}/^{83}\mathrm{Kr})_a = 0$ eqn (2) can be simplified as

$$\left(\frac{^{81}\mathrm{Kr}}{^{83}\mathrm{Kr}}\right)_c = \frac{\left(\frac{^{81}\mathrm{Kr}}{^{83}\mathrm{Kr}}\right)_m \times \left(\frac{^{86}\mathrm{Kr}}{^{83}\mathrm{Kr}}\right)_a}{\left(\frac{^{86}\mathrm{Kr}}{^{83}\mathrm{Kr}}\right)_a - \left(\frac{^{86}\mathrm{Kr}}{^{83}\mathrm{Kr}}\right)_m} \quad (3)$$

Results are reported in Table 2. All uncertainties correspond to one sigma error. Taken into account two-sigma errors, absolute cosmogenic concentrations of ^{83}Kr as well as isotope ratios show good agreement.

Cosmogenic ratios can be used to determine cosmic ray exposure age (T_{81}) of the meteorite,[5] according to the following formula:

$$T_{81} = \frac{T_{1/2}}{\ln(2)} \frac{\left(\frac{P_{81}}{P_{83}}\right)}{\left(\frac{^{81}\mathrm{Kr}}{^{83}\mathrm{Kr}}\right)_c} \quad (4)$$

where $T_{1/2} = 2.29 \times 10^5$ year is the half-live of the ^{81}Kr radionuclide and P_{81}/P_{83} is the ratio of the production rates. This ratio can be deduced from the production ratio of the other isotopes based on the measured ratios and is given by:[24]

$$\frac{P_{81}}{P_{83}} = \frac{0.95}{2}\left(\left(\frac{^{80}\mathrm{Kr}}{^{83}\mathrm{Kr}}\right)_c + \left(\frac{^{82}\mathrm{Kr}}{^{83}\mathrm{Kr}}\right)_c\right) \quad (5)$$

Table 2 Cosmogenic composition in the Boguslavka meteorite. Uncertainties correspond to one sigma error

Sample	Method	^{83}Kr[a]	^{78}Kr/^{83}Kr	^{80}Kr/^{83}Kr	^{81}Kr/^{83}Kr	^{82}Kr/^{83}Kr	^{84}Kr/^{83}Kr	T_{81} (Ma)
Bogu 2.3	MS	1.935	0.3431	0.668	0.00493	0.894	0.172	49.7
		±0.080	±0.0051	±0.011	±0.00029	±0.021	±0.034	±3.0
Bogu 3.1	MS	1.825	0.3463	0.6714	0.00440	0.8740	0.100	55.1
		±0.076	±0.0045	±0.0062	±0.00017	±0.0065	±0.032	±2.2
Bogu 4	RIS-TOF	2.05	0.383	0.715	0.00421	0.900	0.025	60.1
		±0.21	±0.021	±0.027	±0.00051	±0.016	±0.025	±7.0

[a] Absolute concentrations in 10^{-12} cm^3 g^{-1} STP.

In formula (5), the constant 0.95 (interpolation parameter) is established for meteoritic material (essentially SiO_2) under energetic galactic cosmic rays. For metallic media, such studies do not exist except for irradiation of large iron bodies (radius of 10 cm) by 1.6 GeV protons to simulate irradiation by galactic cosmic rays.[25] In this experiment, Kr production rates have been measured in pure Sr, Y and Zr target elements *versus* depth. For the three elements, the interpolation ratio does not evolve in the sphere, and the mean values are 0.90, 0.96 and 0.96 respectively. For iron meteorites, a value of 0.95 is adopted for the calculation with 3% of relative uncertainty (one sigma) because Zr is an important target for Kr production. Ages calculated with formulae (4) and (5) are reported in Table 2. Ages measured using the two techniques are in good agreement. They are also consistent with the age of 63 ± 3 Ma determined using the cosmogenic isotopes ^{39}Ar and ^{38}Ar.[26]

4. Conclusions

A new RIS-TOF facility, FAKIR, has been developed in order to measure Kr isotope abundances with an extremely high sensitivity. The instrument uses Kr resonance ionization with a "2 + 1" ionization scheme and single color UV photons at 216.6 nm. An ion selection system has been added allowing the deflection of any Kr isotope before impacting the detector to prevent blind effect that could alter the detection of the less abundant isotopes. The detection limit of the instrument is 1500 atoms of ^{81}Kr. Operating tests have been successfully performed by analyzing small samples from the Boguslavka iron meteorite using both FAKIR (with few tens mg) and a conventional mass spectrometer (with ~0.7 g samples). A good agreement is observed between the two techniques for measurement of the cosmic ray exposure age of the Boguslavka meteorite. Analysis with FAKIR was performed with only ~6700 atoms of ^{81}Kr. An optimization of the design of the source is in progress. It should improve the focus of the beam leading to better transmission. Furthermore, the sensitivity and the signal to noise ratio should be improved in particular for the less abundant isotopes ^{81}Kr and ^{85}Kr. Beyond its usefulness to study cosmic ray exposure history for different meteorite types (irons, mesosiderites, pallasites, eucrites, chondrites), the measurement of the radioactive krypton isotopes by FAKIR will also be utilized for groundwater and ice core samples dating purposes.

Acknowledgements

This work is financially supported by the CNRS/University of Bordeaux, the Aquitaine region and the CEA/DAM.

References

1 H. H. Loosli and H. Oeschger, *Earth Planet. Sci. Lett.*, 1969, **7**, 67–71.
2 H. Oeschger, *Nucl. Instrum. Methods Phys. Res., Sect. B*, 1987, **29**, 196–202.
3 P. Collon, T. Antaya, B. Davids, M. Fauerbach, R. Harkewicz, M. Hellstrom, W. Kutschera, D. Morrissey, R. Pardo, M. Paul, B. Sherrill and M. Steiner, *Nucl. Instrum. Methods Phys. Res., Sect. B*, 1997, **123**, 122–127.
4 J. N. Andrews, T. Florkowski, B. E. Lehmann and H. H. Loosli, *Appl. Geochem.*, 1991, **6**, 425–434.
5 K. Marti, *Phys. Rev. Lett.*, 1967, **18**, 264–266.
6 O. Eugster, G. F. Herzog, K. Marti, M. W. Caffee and H. Y. McSween, in *Meteorites and the Early Solar System II*, ed. D. S. Lauretta, 2006, pp. 829–851.
7 S. D. Kramer, C. H. Chen, M. G. Payne, G. S. Hurst and B. E. Lehmann, *Appl. Opt.*, 1983, **22**, 3271–3275.
8 B. E. Lehmann, H. Oeschger, H. H. Loosli, G. S. Hurst, S. L. Allman, C. H. Chen, S. D. Kramer, M. G. Payne, R. C. Phillips, R. D. Willis and N. Thonnard, *J. Geophys. Res.*, 1985, **90**, 11547–11552.
9 I. Strashnov, D. J. Blagburn, N. Thonnard and J. D. Gilmour, *Opt. Commun.*, 2009, **282**, 966–969.
10 I. Strashnov and J. D. Gilmour, *Meteorit. Planet. Sci.*, 2013, **48**, 2430–2440.
11 B. Lavielle, B. Thomas, E. Gilabert, G. Canchel, C. Moulin, S. Topin and F. Pointurier, *J. Mass Spectrom.*, 2016, submitted.
12 N. Thonnard, R. D. Willis, M. C. Wright, W. A. Davis and B. E. Lehmann, *Nucl. Instrum. Methods Phys. Res., Sect. B*, 1987, **29**, 398–406.
13 J. D. Gilmour, I. C. Lyon, W. A. Johnston and G. Turner, *Rev. Sci. Instrum.*, 1994, **65**, 617–625.
14 I. Strashnov, D. J. Blagburn and J. D. Gilmour, *Lunar Planet. Sci.*, 2010, **41**, 1708.
15 I. Strashnov, D. J. Blagburn and J. D. Gilmour, *J. Anal. At. Spectrom.*, 2011, **26**, 1763–1772.
16 K. Watanabe, T. Iguchi, T. Ogita, A. Uritani and H. Harano, *J. Nucl. Sci. Technol.*, 2001, **38**, 844–849.
17 G. S. Hurst, M. G. Payne, R. C. Phillips, J. W. T. Dabbs and B. E. Lehmann, *J. Appl. Phys.*, 1984, **55**, 1278–1284.
18 B. E. Lehmann, H. H. Loosli, H. Oeschger, D. Rauber, G. S. Hurst, S. L. Allman, C. H. Chen, S. D. Kramer, N. Thonnard and R. D. Willis, *Radiocarbon*, 1986, **28**, 223–228.
19 D. Porcelli, C. J. Ballentine and R. Wieler, *Rev. Mineral. Geochem.*, 2002, **47**, 1–19.
20 NIST, http://www.physics.nist.gov/PhysRefData/ASD, 2014.
21 I. Strashnov, D. J. Blagburn and J. D. Gilmour, *Opt. Commun.*, 2009, **282**, 3487–3492.
22 B. Lavielle, S. Toe and E. Gilabert, *Meteorit. Planet. Sci.*, 1997, **32**, 97–107.
23 K. Marti, P. Eberhardt and J. Geiss, *Z. Naturforsch., A: Astrophys., Phys. Phys. Chem.*, 1966, **21**, 398.
24 A. Shukolyukov and F. Begemann, *Meteorit. Planet. Sci.*, 1996, **31**, 60–72.
25 E. Gilabert, B. Lavielle, R. Michel, I. Leya, S. Neumann and U. Herpers, *Meteorit. Planet. Sci.*, 2002, **37**, 951–976.
26 A. V. Fisenko, V. A. Alekseev and L. K. Levskii, *Meteoritika*, 1979, **38**, 59–61.